BioGecko Vol 12 Issue 03 2023

ISSN NO: 2230-5807

LUNG CANCER DETECTION USING AI

Jakka RajKumar[1], Sree RamaKavacham srichandu[2], B.M.S.M. Durga Prasad[3], Chava Hemanth Thilak[4], K.Baalaji [5]*

Department Of Computer Science and Engineering, Bharath Institute of Science & Technology affiliated to Bharath Institute of Higher Education and Research, Chennai, Tamilnadu, India.

*Corresponding authors mail id: baalaji.cse@bharathuniv.ac.in

ABSTRACT

The battle against cancer is challenging for all medical professionals and researchers. The best chance of saving lives is early identification of most malignancies. This research suggested a VEE NET-based deep learning method for lung cancer diagnosis. For the many sorts of cancer diagnostics on this project, visual inspection and manual procedures are applied. This manual evaluation of scientific photographs requires a significant time commitment and is very prone to error. So, in this study, we use deep learning algorithms to detect the existence of lung cancer without the need for several medical visits. As a result, the illness may be predicted early, enabling us to intervene sooner to stop its progression while minimizing the risk of human mistake and a web-based healthcare application capable of detecting lung cancer from an x-ray image.

Keywords: *Computed Tomography (CT), X-ray, Tumor, Lung Cancer, CLAHE, Chest, Accuracy.*

1. INTRODUCTION

Cancer in lungs, known as lung carcinoma. An uncontrolled growth of cells in lung tissues can lead to metastases spreading to surrounding tissue or to other parts of the body, causing this type of malignant lung tumor to grow beyond lung tissue [1]. The majority of primary lung malignancies, also known as twitching tumors, are carcinomas. Common symptoms include a chronic cough, weight issues, shortness of breath, and chest, shoulder, and arm discomfort. Around 85 percent of all persons will develop lung cancer due to their lifetime of smoking. Around 10 to 15 percent of possessions belong to persons who don't smoke [2]. These traits are typically a result of a genetic predisposition combined with exposure to air pollution, whether from radon gas, asbestos, second hand smoking, or anything else. Computed Tomography (CT) images obtained during a chest x-ray are used to diagnose lung cancer [3]. The diagnosis is confirmed with a biopsy, which is often performed under bronchoscopy or CT guidance over 1.8 million patients worldwide were afflicted with lung cancer in 2012, while 1.6 million people passed away from the disease [4]. Lung cancer affects around 20% of the population in general [5]. The survival rate after an illness has been present for five years is very low, and results are often worse in the developing countries. A ridge regression approach is used for the same and further discussed in this article; we provide segmentation of image analysis as a method for detecting non-invasive anaemia [6]. Treatment of lung cancer using stereotactic body radiation therapy is presented, along with the use of unsupervised prediction based on image analysis performed in Matlab [7]. Medical images employ edge vectors and mapping to locate boundaries. When it comes to security systems and fingerprint vein analysis, an image retrieval strategy based on content is developed to help with texture and shape analysis [8]. In addition to utilising CT to classify nodules in thorax pictures using SVM, detecting lung cancer using CT images is covered in. In this article, we provide segmentation of image analysis as a method for detecting non-invasive anaemia [9]. Treatment of lung cancer using stereotactic body radiation therapy is presented, along with the use of unsupervised prediction based on image analysis performed in Matlab. Medical images employ edge vectors and mapping to locate boundaries. When it comes to security systems and fingerprint vein analysis, an image retrieval strategy based on content is developed to

help with texture and shape analysis [10]. Clinical and radiomic characteristics were used to diagnose lung cancer, and CT-based image analysis was used to predict lung adenocarcinoma. Lung cancer also has one of the largest financial burdens on society globally. After undergoing chemotherapy and radiation treatment, most patients expect to live 14 months after diagnosis, with a monthly cost of $400 to $8,000. Every 100,000 people in Europe are estimated to be affected by lung cancer [11]. Its annual healthcare and patient management expenses are anticipated to be 17,000 Euros.

In a high-risk group, low-dose computed tomography (LDCT) examinations were shown to result in a 20% lower death rate than routine chest X-rays. Moreover, low-dose of CT has a detection rate for lung cancer screening that is 2.6 to 10 times greater than chest radiography. Early diagnosis is the key to lowering lung cancer-related fatalities, and this depends on quick and accurate lung nodule identification and meticulous chest CT scan inspection to confirm malignancy processes that take radiologists and doctors a lot of time and effort to complete.

Studies show that general practitioners and specialists alike often spend up to twice as much time on paperwork as they do with patients. They then put in another hour or two of work following clinic, primarily utilizing the electronic medical record [12]. Patients with lung cancer at risk should be screened by the clinicians, the time required to examine and process CT images is substantially higher for them.

Dr. Flanou oncologist stated with a reported prevalence between 35 and 60%, are more at risk from burnout compared to other. Twenty percent to thirty five percent of people who experience burnout are at risk for mental health problems, and burnout is also indirectly related to a decrease in empathy among doctors as well as in the quality of care they provide they provide their patients. As both patients and doctors benefit from reduced workloads, it is important to investigate all possibilities.

The use of artificial intelligence (AI) for automated CT lung cancer diagnosis is one such solution that could be implemented to assist physicians in reducing their caseloads, enhancing hospital patient care workflow, and giving up more satisfactory time for them to cultivate meaningful relationships with their patients. To diagnose benign or malignant lung cancer changes, gather and analyse data from CT scans, and screen patients using 3D CT scans, Niki et al. initiated computer-aided detection (CAD). It was found that CAD improved the performance of radiologists when diagnosing small lung nodules, around 5 mm in diameter, which are difficult to detect visually. Hence, CAD and the accompanying when lung cancer is diagnosed early, when nodules are more likely to go undetected, AI can improve diagnosis. This is because they reduce the stress on clinicians and, thus, fatigue-related mistakes of judgment.

2. METHODOLOGY

2.1. VGG-16

The Image Net Large Scale Visual Recognition Competition (ILSVRC) is an annual computer vision contest. This crew competes in two events. Object localization is the initial phase, and it includes identifying things in an image that belong to one of 200 classes. In a second stage, classifying pictures entails assigning each photo to one of a thousand different classes. Karen Simonyan and Andrew Zisserman of the Visual Geometry Group Lab at Oxford University introduced VGG 16(figure 1) in their 2014 paper "VERY DEEP CONVOLUTIONAL NETWORKS FOR LARGE-SCALE IMAGE RECOGNITION."

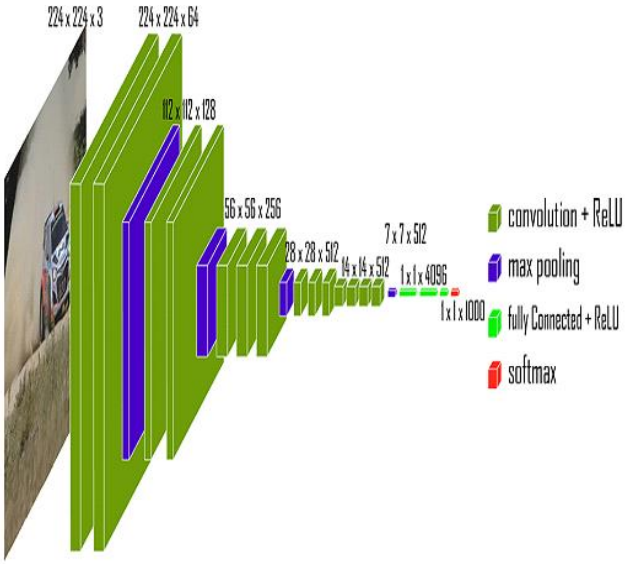

Figure 1. Architecture of VGG - 16

In figure 1, when tested on the ImageNet dataset, which contains 14 million images labeled with one thousand classes, 92.7% of the tests are accurate with this model. The Image Net collection consists of pictures having color space of RGB and dimension of 224x224 pixels. Our input is hence a tensor of (224, 224, and 3). This model examines the given picture and returns a 1000-valued vector for analysis.

$$\hat{y} = \begin{bmatrix} \hat{y_0} \\ \hat{y_1} \\ \hat{y_2} \\ \hat{y_3} \\ . \\ . \\ . \\ . \\ \hat{y_{999}} \end{bmatrix}$$

(equation 1)

Probability of placing a given class may be expressed as a vector, which is what we've done here. A model could say an image is most likely to be in class 0 (with a probability of 1), classes 1 and 2 (with a probability of 0.5), classes 3 (with probabilities of 0.03), classes 780 and 999 (with probabilities of 0.72 and 0.05, respectively), and all other classes (with a probability of 0). You may use the following vector to categorize this:

$$\hat{y} = \begin{bmatrix} \hat{y_0} = 0.1 \\ 0.05 \\ 0.05 \\ 0.03 \\ . \\ . \\ . \\ \hat{y_{780}} = 0.72 \\ . \\ . \\ \hat{y_{999}} = 0.05 \end{bmatrix}$$

(equation 2)

To ensure that the total of these probabilities equals 1, we use the soft max function. Five of the most likely choices are then entered into the vector.

$$C = \begin{bmatrix} 780 \\ 0 \\ 1 \\ 2 \\ 999 \end{bmatrix}$$

(equation 3)

This is how we characterize the ground truth vector value:

$$G = \begin{bmatrix} G_0 \\ G_1 \\ G_2 \end{bmatrix} = \begin{bmatrix} 780 \\ 2 \\ 999 \end{bmatrix}$$

(equation 4)

Our Error function is therefore defined as follows:

$$E = \frac{1}{n} \sum_k min_i d(c_i, G_k) \quad (5)$$

If c {i} is equal to G k, then d is zero; otherwise, d is one. This particular loss function looks like this:

$$E = \frac{1}{3}\left(min_i d(c_i, G_1) + min_i d(c_i, G_2) + min_i d(c_i, G_3)\right) \quad (6)$$

So,

$$E = \frac{1}{3}(0 + 0 + 0) \quad (7)$$

It goes like this: [Tex] kern 6pc E, =, 0 [/Tex] As a result of all ground-truth categories being included in the Expected top-5 matrix, the loss is now at zero.

In the VGG Architecture, a dimensioned picture serves as the network's input (224, 224, 3). The first two tiers have 64 channels, each with a 33 pixel filter size and the same padding. Layers of convolution with 128- and 256-pixel filters follow a max pool layer of stride (2, 2) in the network's architecture (3, 3). Next is a layer of stride (2, 2) max-pooling, which is otherwise similar to the previous layer. The subsequent two convolution layers each include 256 filters with a 3x3 filter size. Then comes a max pool layer, then a trio of convolution layers in two distinct groups of three. Each has 512 filters with the same padding and size (3, 3). Afterwards, the image is sent on to a stack of two convolution layers. Our convolution and max-pooling layers use 3*3 filters, while AlexNet and ZF-Net use 11*11 and 7*7, respectively. The number of input channels may be adjusted by replacing some of the layers with ones consisting of only 1*1 pixels. After each convolution layer, 1-pixel padding is utilized to mask the image's spatial feature.

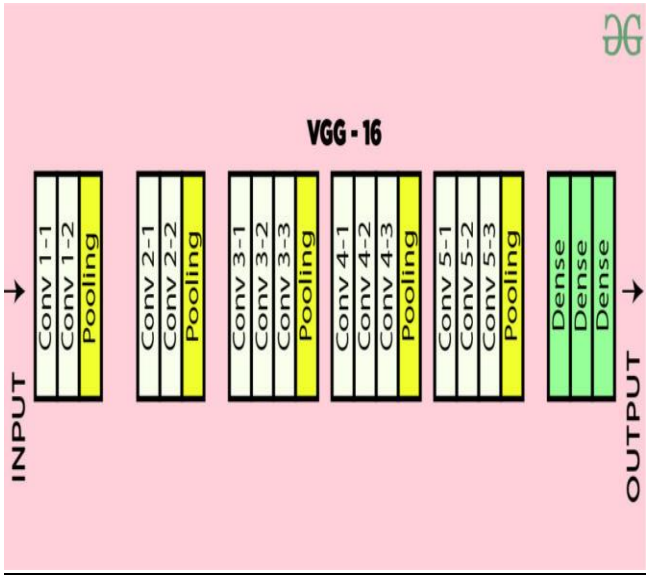

Figure 2. VGG-16 architecture convolution layers

Convolution followed by max-pooling was used to generate the (7, 7, 512) feature map as shown in figure 2. As a consequence, we flatten the result into a (1, 25088) feature vector. Following then, there are three distinct yet interconnected levels: the first layer uses the output of the previous layer's features The first layer feeds its output into the second layer, which then feeds its output into the third layer to produce a (1, 4096) vector to generate a vector with 1,000 channels, one for each of the 1,000 classes in the ILSVRC challenge. All the buried layer's active functions are ReLU. Because of its quicker learning and ReLU is more computationally efficient for the probability of lower vanishing gradient problems. The various VGG configurations are shown in table 1 below. Two distinct forms of VGG-16 have been identified C and D. The latter uses (3, 3) filter size convolution for all but a few convolution layers, and that's the only meaningful difference (1, 1). These two have a total of 138 million parameters and 134 million, respectively.

ConvNet Configuration					
A	A-LRN	B	C	D	E
11 weight layers	11 weight layers	13 weight layers	16 weight layers	16 weight layers	19 weight layers
input (224 × 224 RGB image)					
conv3-64	conv3-64 **LRN**	conv3-64 **conv3-64**	conv3-64 conv3-64	conv3-64 conv3-64	conv3-64 conv3-64
maxpool					
conv3-128	conv3-128	conv3-128 **conv3-128**	conv3-128 conv3-128	conv3-128 conv3-128	conv3-128 conv3-128
maxpool					
conv3-256 conv3-256	conv3-256 conv3-256	conv3-256 conv3-256	conv3-256 conv3-256 **conv1-256**	conv3-256 conv3-256 **conv3-256**	conv3-256 conv3-256 conv3-256 **conv3-256**
maxpool					
conv3-512 conv3-512	conv3-512 conv3-512	conv3-512 conv3-512	conv3-512 conv3-512 **conv1-512**	conv3-512 conv3-512 **conv3-512**	conv3-512 conv3-512 conv3-512 **conv3-512**
maxpool					
conv3-512 conv3-512	conv3-512 conv3-512	conv3-512 conv3-512	conv3-512 conv3-512 **conv1-512**	conv3-512 conv3-512 **conv3-512**	conv3-512 conv3-512 conv3-512 **conv3-512**
maxpool					
FC-4096					
FC-4096					
FC-1000					
soft-max					

Table 1. Different VGG Configuration

In order to carry out localization, the class score must be exchanged for bounding box position coordinates. The four-dimensional vector (x, y, height, width) of a bounding box's location is used to express the location's extents. One type of localization architecture has a common bounding box for all candidates (with a 4 parameter vector as output), whereas the other type has each kind has its own specific boundary box (the output is 4000 parameter vector). Both methods were tested on the VGG -16 architecture used in this work. In this case, an appropriate regression loss function that penalizes the difference between the expected loss and the actual loss should be used rather than a classification loss (like mean squared error).

VGG-16's results showed that it was among the top-performing designs in the 2014 ILSVRC competition. With a classification error in the top five (only behind Google Net's 6.66%) it placed second in the classification challenge. It also triumphed in the localization competition, with an error rate of only 25.32 percent.

The training speed of VGG 16 is really low and the first VGG model required two to three weeks of training on an NVidia Titan GPU. The 528 MB in size is the trained image Net weights for VGG-16. Thus, it is inefficient since it requires high memory capacity and transmission speed. The problem of expanding gradients arises when there are 138 million parameters. The ballooning gradients issue that plagued VGG-16 was addressed with the introduction of Resents, which represented another step forward.

2.2. MODUELS

2.2.1. Dataset

As part of the current effort, a new image collection comprising X-ray and CT scans has been made accessible to the general public. Here is a link to a dataset including 5856 pictures in jpeg format and it is called as the chest X-ray and CT dataset. There are two distinct sets of images as 4273 pneumonia and 1583 normal. Chest X-ray examples are shown in Figure 3, the lungs should be transparent on a chest X-ray taken from an individual suffering from pneumonia. However, whereas most of the lungs exhibit a pattern of focal lobar consolidation (white arrows), two of the lungs exhibit a more widespread "interstitial" pattern.

Figure 3. Chest X –RAY

2.2.2 Data Splitting and preprocessing

The following step involves preparing the input photos using a variety of pre-processing methods. Improved visual information quality is the driving force behind image pre-processing by delete the low or high frequencies, raise the contrast, or remove noise from the original input picture. Here, we employed contrast-limited adaptive histogram equalization and intensity normalization (CLAHE). As a preliminary technique for image processing, intensity normalization is worth exploring (Kassani et al., 2019). By employing min-max normalization, we standardised the input pictures used in our models (Figure 4. (a)) to the normal distribution (Equation1). Moreover, CLAHE is required to enhance picture contrast before to feeding input photos into the suggested models depicts use of these methods.

$$X_{norm} = \frac{x - x_{\min}}{x_{\max} - x_{\min}} \quad (8)$$

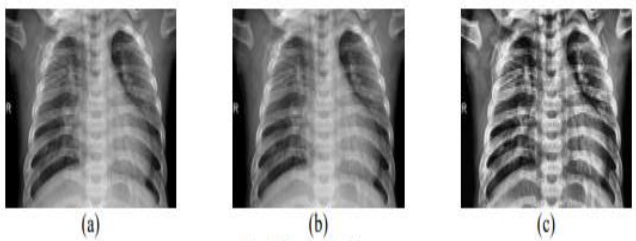

Figure 4. Using CLAHE Techniques to Improve Image contrast

Here, Sixty percent of the images were utilized for training, while the remaining forty percent were used for validation with the data divided in between. We successfully complete the binary classification job by avoiding the usage of the validation pictures during training. In addition, we found that our dataset is skewed, with 75% of the photos belonging to the pneumonia category. Our dataset was resampled via data augmentation so that we could get around this problem. Two new photos, enhanced in two distinct ways, were really created from each original input image. Hence, the sum of photos in the usual class was doubled.

2.2.2. Data augmentation

When the dataset has been pre-processed and partitioned, data augmentation (table 2) is utilized in the training phase to reduce the likelihood of over fitting. In addition, we employed techniques including resizing, rotations, shifts, shears, zooms, and flips as part of a larger set of geometric transformations.

Argument	Parameter value	Description
Rescale	1 / 255.0	Scale images from integers 0-255 to floats 0-1
Rotation range	90	Degree range of the random rotations
Vertical shift range	0.2	The parameter value of horizontal and vertical shifts (20%) is a fraction of the given dimension
Horizontal shift range	0.2	
Shear range	0.2	Controls the angle in counterclockwise direction as radians in which our image will allowed to be sheared
Zoom range	0.2	Allows the image to be "zoomed out" or "zoomed in"

Table 2. Augmentation done to avoid data over fitting

2.2.3. Training and classification dataset

Training Methods is the initial step of this technique is for the purpose of model training through image enhancement. As a result of this image enhancement, we can quickly and effectively Using the data set as a training set, preprocess all the images and convert them into a large number of images with varying viewpoints. Many methods are detailed below like array pre-processing, rotation, flipping, etc., components of our education. By combining the two deep learning frameworks, VGG-16 and Resnet-75, after the datasets have been enhanced, they may be trained. It goes through a process termed optimisation, which improves loss minimization, which seeks to reduce the model's noise output as much as possible during training. Finally, the generated model will be tested on a dataset meant for predicting the existence of lung cancer, a procedure known as seriation matrices. After that, the python programs are run in the visual studio environment. The training procedure in the proposed system is depicted as a flowchart in figure 4. Dataset acquisition, pre-processing, partitioning, training, and testing using VGG-16 are the training process components illustrated. By iteratively optimizing, validating, and evaluating, we achieve the best possible result.

2.2.4. Experimental setup

Our experiments using as open to the public picture the Chest X-Ray dataset aimed to automatically classify the images into one of two categories. Except for the photos associated with the Inception V3 model, which were downsized to 299x299. We use 32-sample batches and 300-iteration epochs to hone our models. Sample sizes for

training and testing have been chosen at 159 and 109, respectively. The learning rate is first set at 0. 00001 and then decreased to 0.000001 when Adam is used for optimization with 1=0.9 and 2=0.999. To avoid this, we used weight decay in our models. Under keras, you'll find the regularizes known as L2. Microsoft Windows 10 Professional is installed on a machine with an Intel (R) core (TM) i7-7700 CPU operating at 3.60 GHz and 8 GB of RAM, where the recommended models have been developed (64-bit). Keras/tensor flow is used as the deep learning backend, while Python 3 is used for simulation. NVIDIA Tesla P40s with 24 GB of RAM power are the training and certification procedures.

2.2.5. Evaluation criteria

The final step is classifying the obtained data and assigning it to a certain class after the suitable feature has been extracted (Blum et al., 2001). Accuracy, sensitivity, specificity, precision, and F1 score are used as benchmarks in our study as they represent various classification performance features and our data is well-balanced. The following are the definitions of several well-known values:

$$Accuracy = \frac{TP+TN}{TN+TP+FP+FN}$$

$$Sensitivity = \frac{TP}{TP+FN}$$

$$Specificity = \frac{TN}{TN+FP}$$

$$Precision = \frac{TP}{TP+FP}$$

$$F1 = 2 \times \frac{Recall \times precision}{Recall + precision} \quad (9)$$

3. RESULTS AND DICUSSION

After a run of the deep learning algorithm is complete, it produces an accuracy plot for the training. The proposed model is straightforward to implement and tackles the system's doubtful accuracy and the complexity of the real-time operation head-on. With the suggested method, the presence of cancer may be discovered at an early stage, which is not possible with the current set of diagnostic markers for the disease [2]. Although current methods of cancer-image detection fall short of expectations, a system built with a deep learning algorithm achieves pinpoint precision. After training, a graph validating accuracy and a picture of the training loss are used to make an evaluation. Loss was greater and accuracy was worse in the initial training phase. By going through the training procedure again, we were able to improve our accuracy and cut down on our loss. Accuracy for the training with the deep learning method is displayed as the execution progresses. The suggested model overcomes the system's low accuracy and the real-time process's complexity, both of which are mentioned in [1], through its simplicity and precision in implementation. It is impossible to identify cancer using the current set of diagnostic tools [2], but the suggested approach would allow for early detection of the disease. In contrast to the unsatisfactory performance of previously used methods, the system constructed using a deep learning algorithm is 100% accurate when used to the detection of images for cancer diagnosis. After training, a graph validating accuracy and a picture of the training loss are used to make an evaluation as shown in

table 3. Accuracy suffered and losses increased in the first training phase. By further training it was possible to improve accuracy and decrease loss.

	Precision	Recall	F1-score	Support
Ignore	1.00	1.00	1.00	34
Lung_cancer	1.00	1.00	1.00	27
Lung_normal	1.00	1.00	1.00	49
Accuracy			1.00	110
Macro Average	1.00	1.00	1.00	110

Table 3. Evaluation Criteria

The file will also automatically save the model's learned graph.

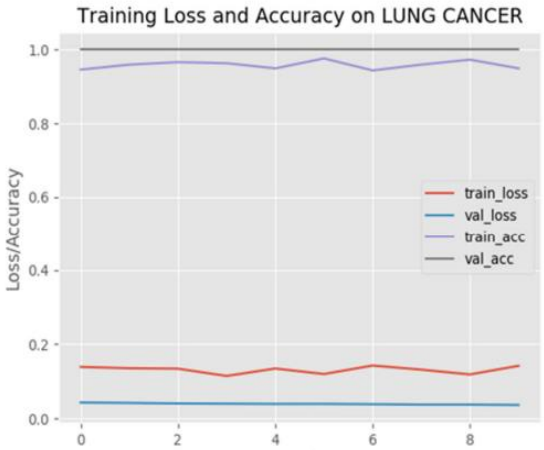

Graph 1. Training Model Validation Graph

We used transfer learning of modern deep learning architectures to classify X-ray pictures into two categories: normal and pneumonia. This allowed us to determine which design performed best given the various parameters described by equation2. To begin, we use accuracy measurements to directly compare the various deep learning techniques. Following that, we determine whether DL architecture is superior by comparing the accuracy and loss outcomes it produces. Using the parameters specified by equation2, which shows how our various deep learning models performed in our experiment. When measuring training and validation accuracy over the course of several epochs, the fine-tuned versions of Inception Resnet V2, Inception V3, Resnet50, DenseNet201, and Mobilenet V2 are found to perform well. In terms of performance, they are superior to Xception, VGG16, and VGG16 all outperformed the poorly performing baseline CNN. Accuracy in training and validation for baseline CNN, VGG16, and VGG16 is 85%, at Training finishes around epoch 20, when it begins to stabilize. The validation accuracy of Xception is 83%, whereas the training accuracy is 95%. The Xception-generated prediction model does not suit the training Set very well in this instance (Over fiting). In addition, each suggested model reaches a point of stability as shown by the training and validation loss plots in graph 1 be observed, our models function admirably after being fine-tuned, as seen by the steady

improvement in both training and validation loss over time. The table shows the categorization results for each experiment in great detail. Notable from the outcomes is the accuracy achieved by using baseline CNN, Xception, and VGG16.

In the realms of image processing and computer vision, recent advances in AI techniques have shown immense promise. These methods have shown promising results in the fields of medical imaging segmentation, detection, and classification when applied to a variety of imaging modalities. Cancers like as skin cancer, breast cancer, lung cancer, etc. may all be detected and classified by some AI algorithms. Although these techniques have demonstrated remarkable effectiveness in medical imaging, they need a vast amount of data that is currently lacking in this area of application. In this study, we will use Transfer learning to fine-tune the top layer of the following AI architectures (CNN, VGG16) and diagnose illness in a setting when there is no medical imaging dataset available.

The suggested system's strength lies in the fact that the VGG16 model can accomplish 92.7% test accuracy in CNN. More than 14 million photos from 1,000 different item classifications make up this collection. It's a top contender from the ILSVRC-2014 contest. To make improvements over CNN, VGG16 uses a series of smaller 33 filters instead of a single huge filter.

To increase the effectiveness of CAD with CT for lung cancer screening, we have been experimenting with many deep learning methods. Here, we provide an implementation of pre-trained Convolutional Neural Networks, which are utilised both in network training and CT image categorization. High performance and precision in lung cancer identification on CT images are achieved using CNN and TL. Model quality may be measured with the use of a number of different matrices, including the confusion matrix, accuracy, recall, specificity, and f1-score.

Disadvantages include high prices (depending on the chosen system and the number of detectors), lengthy processing times, and a dearth of suitably trained personnel and data. Training data for machine learning algorithms must be large, diverse, and accurate.

4. CONCLUSION

In this study, lung cancer was detected in its earliest stages. VGG is employed, which is 16-layer architecture. In order to get the most precise results, the input is run through all 16 levels. Other architectonics can be compared to VGG, or more convolutional layers can be added to improve accuracy and likelihood of success. In this study, we presented nine different the focus here is on resolving a particular research puzzle. Is there one DCNN method that trumps all the others when it comes to accuracy and speed? A total of 5856 images from chest X-rays and CT scans were used in the studies (4273 pneumonia and 1583 normal) and the results were analyzed using a number of different performance indicators. As compared to previous designs referenced in this work accuracy is approximately 84%, the findings demonstrate that the Resnet50, MobileNet V2, and Inception Resnet V2 delivered highly performance accuracy is more than 96%. Current efforts aim to create a comprehensive system for identifying and categorizing cases of pneumonia using deep learning

REFERENCES

[1] O. Russakovsky et al., “ImageNet Large Scale Visual Recognition Challenge,” Int. J. Comput. Vis., vol. 115, no. 3, pp. 211–252, 2015, doi: 10.1007/s11263-015-0816-y.

[2] S. J. Pan and Q. Yang, “A survey on transfer learning,” IEEE Trans. Knowl. Data

[3] G. E. H. Alex Krizhevsky, Ilya Sutskever, “Handbook of approximation algorithms and metaheuristics,” Handb. Approx. Algorithms Metaheuristics, pp. 1–1432, 2007, doi: 10.1201/9781420010749.

[4] V. Sangeetha and K. J. R. Prasad, “Syntheses of novel derivatives of 2-acetylfuro[2,3-a]carbazoles, benzo[1,2-b]-1,4-thiazepino[2,3- a]carbazoles and 1-acetyloxycarbazole-2- carbaldehydes,” Indian J. Chem. - Sect. B Org. Med. Chem., vol. 45, no. 8, pp. 1951–1954, 2006, doi: 10.1002/chin.200650130.

[5] C. Szeged et al., “Going deeper with convolutions,” Proc. IEEE Comput. Soc. Conf. Comput. Vis. Pattern Recognit., vol. 07-12-June, pp. 1–9, 2015, doi: 10.1109/CVPR.2015.7298594.

[6] E. Cengil and A. Çinar, “A Deep Learning Based Approach to Lung Cancer Identification,” 2018 Int. Conf. Artif. Intell. Data Process. IDAP 2018, 2019, doi: 10.1109/IDAP.2018.8620723. Z. Shi et al., “A deep CNN based transfer learning method for false positive reduction,” Multimed. Tools Appl., vol. 78, no. 1, pp. 1017–1033, 2019, doi: 10.1007/s11042-018-6082-6.

[7] R. Anirudh, J. J. Thiagarajan, T. Bremer, and H. Kim, “Lung nodule detection using 3D convolutional neural networks trained on weakly labeled data,” Med. Imaging 2016 Comput. Diagnosis, vol. 9785, no. November 2017, p. 978532, 2016, doi: 10.1117/12.2214876.

[8] Q. Z. Song, L. Zhao, X. K. Luo, and X. C. Dou, “Using Deep Learning for Classification of Lung Nodules on Computed Tomography Images,” J. Healthc. Eng., vol. 2017, 2017, doi: 10.1155/2017/8314740.

[9] B. S, P. R and A. B, "Lung Cancer Detection using Machine Learning," *2022 International Conference on Applied Artificial Intelligence and Computing (ICAAIC)*, Salem, India, 2022, pp. 539-543, doi: 10.1109/ICAAIC53929.2022.9793061.

[10] F. Taher, "Early detection of lung cancer based on artificial intelligence techniques," *2017 International Conference on Infocom Technologies and Unmanned Systems (Trends and Future Directions) (ICTUS)*, Dubai, United Arab Emirates, 2017, pp. 1-1, doi: 10.1109/ICTUS.2017.8285987

[11] S. Mukherjee and S. U. Bohra, "Lung Cancer Disease Diagnosis Using Machine Learning Approach," 2020 3rd International Conference on Intelligent Sustainable Systems (ICISS), Thoothukudi, India, 2020, pp. 207-211, doi: 10.1109/ICISS49785.2020.9315909.

[12] K. Ingle, U. Chaskar and S. Rathod, "Lung Cancer Types Prediction Using Machine Learning Approach," *2021 IEEE International Conference on Electronics, Computing and Communication Technologies (CONECCT)*, Bangalore, India, 2021, pp. 01-06, doi: 10.1109/CONECCT52877.2021.9622568.